

# **Assembly of dielectric measurement instrument and properties of BaTiO<sub>3</sub> synthesized via hydrothermal route**

A thesis submitted to

**Jawaharlal Nehru University**

In partial fulfilment of the requirements of the degree of

**Master of Technology in Nanoelectronics**

**By**

**Anurag Kumar**

Under the supervision of

**Dr . Balaji Birajdar**

(Assistant Professor, SCNS, JNU, New Delhi)



Special centre for Nanoscience

Jawaharlal Nehru University

New Delhi -110067 ,India

2021

**RECOMMENDATION FORM FOR EVALUTION BY THE EXAMINER**


**CERTIFICATE**

This is to certify the dissertation/thesis titled **"Assembly of dielectric measurement instrument and change in properties of BaTiO3 synthesized via hydrothermal route"** submitted by **Mr. Anurag Kumar** in partial fulfillment of the requirements for award of degree of M.Tech of Jawaharlal Nehru University, New Delhi, has not been previously submitted in part or in full for any other degree of this university or any other university/institution.

We recommend this thesis/dissertation be placed before the examiner for evaluation for the award of the degree of M. Tech.

*B. Prasad*  
19/05/2022

**Signature of the Supervisor**

**Date:**    
 Dr. Anurag Kumar  
 Special Centre for Nano Sciences  
 Jawaharlal Nehru University  
 New Delhi - 110067

*Dr. S. S. Singh*  
19/05/2022

**Signature of the Dean/Chairperson**

**Date:**    
 Dr. S. S. Singh  
 Special Centre for Nano Sciences  
 Jawaharlal Nehru University  
 New Delhi - 110067

## **DECLARATION**

I hereby certify that the work which is being entitled “**Assembly of dielectric measurement instrument and change in properties of BaTiO<sub>3</sub> synthesized via hydrothermal route**” in the fulfilment of the requirement for the degree of Master of Technology in Nano-electronics and submitted to “ Special center for Nanoscience, Jawaharlal Nehru University, New Delhi”, is an authentic record of my work carried out under the supervision of Dr. Balaji Birajdar, Associate Professor SCNS – Jawaharlal Nehru University, New Delhi. The matter presented in this thesis has not been submitted for the award of any other degree/diploma of this institute or any other University.

**Anurag Kumar**

**Dr. Balaji Birajdar**

Assistant Professor

Special Center For Nanoscience

Jawaharlal Nehru University

New Delhi - 110067

**Dr. Satyendra Singh**

Chairperson

Special Center For Nanoscience

Jawaharlal Nehru University

New Delhi - 110067

## **Acknowledgement**

I would like to express my sincere gratitude to my supervisor Dr. Balaji Birajdar for providing his valuable guidance, comments and suggestions throughout the course of project. I greatly appreciate the motivation and understanding he has provided during the project work. I feel privileged for the opportunity of working in such a well-established lab.

I would like to thank Dr. Rohtash for enriching me with his work on dielectric measurement setup through his guidance and thesis work.

I would like to thank PhD scholar Devendra Singh for sharing his knowledge. He has given his guidance for various analytical techniques required for this project work.

I would like to thank my lab mates and seniors for such friendly and supportive atmosphere in the lab. Such welcoming atmosphere has always motivated me throughout the project work.

I would also like to thank my classmates and my friends for their cooperation support in completing my project.

**Anurag Kumar**



## ABSTARCT

In the first chapter I have summarised my work regarding impedance analyser and its set up to obtain dielectric properties using a temperature controller and LABVIEW program. My work is based on the thesis of Dr. Rohtash, SCNS, JNU for assembly of the system that I couldn't finish due to Covid. From start I have described the working theory which is based upon the values of real and imaginary impedance parameters to realise the permittivity. The main component is sample holder which is used in measurement is described and connections are also mentioned briefly. Vaccum system is very essential for the measurement and application of LABIEW program is shown which articulate the whole experiment by creating an interface.

In the second chapter, Nanoparticles of BaTiO<sub>3</sub> were synthesized via hydrothermal route to study the properties. Low temperature (at 180° C) synthesis provides an alternate route for homogeneity, less energy consumption, high stoichiometric accuracy. The material obtained contains mixed phase constituting of tetragonal and cubic structure. There can be presence of certain impurities like BaCO<sub>3</sub> and TiO<sub>2</sub> depending upon the degree of reaction, temperature etc. The synthesized BaTiO<sub>3</sub> is having phases corresponding to cubic and tetragonal can be determined using Xrd and Raman plot. The splitting of the (200) peak at  $2\theta = 45.37^\circ$  into two peaks (002) and (200) shows mixed phase. Raman shift peak about 300 cm<sup>-1</sup> starts to diminish while reaching Curie temperature and transition to cubic phase.

## Table of contents

Acknowledgement

Abstract

List of tables

List of figures

Chapter 1 – Introduction for dielectric measurement.....	1
1.1 Impedance spectroscopy .....	1
1.2 Specification required for the assembled instrument .....	3
1.3 Assembly of liquid nitrogen system .....	3
1.4 Design and construction of sample holder of lower section .....	4
1.5 Vacuum system accessory .....	4
1.6 Measurement procedure for dielectric properties .....	5
1.7 LABVIEW Program .....	5
Chapter 2 – Introduction for BaTiO <sub>3</sub> synthesis .....	6
2.1 Perovskite structure .....	7
2.1.1 Causes of distortion .....	8
2.1.1.1 Tolerance effect .....	8
2.1.1.2 Jahn-Teller effect .....	8
2.2 Polarization .....	8
2.2.1 Types of polarization .....	9
2.2.1.1 Electronic Polarization .....	9
2.2.1.2 Atomic or Ionic polarization .....	10
2.2.1.3 Orientation Polarization .....	11
2.2.1.4 Spontaneous Polarization .....	11

2.2.1.5 Space charge polarization .....	12
2.3 Ferroelectricity .....	13
2.3.1 Distortion in cubic structure to attain ferroelectricity .....	13
2.3.1.1 Displacement of B cations .....	13
2.3.1.2 Tilt in octahedral geometry .....	13
2.3.1.3 Octahedral distortion .....	13
2.3.2 Domains .....	14
2.4 Piezoelectricity .....	15
2.5 Literature review of BTO .....	17
2.5.1 Structure and phase of BaTiO <sub>3</sub> .....	17
Chapter 3 - Synthesis of BaTiO <sub>3</sub> .....	19
3.1 Hydrothermal method .....	19
3.2 Experimental synthesis .....	19
Chapter 4 – Characterization .....	21
4.1 X-ray Diffraction .....	21
4.2 Raman Spectroscopy .....	22
4.3 Dielectric measurement.....	24
Chapter 5 - Results and discussion .....	25
5.1 Structural study .....	25
5.2 Raman study .....	26
5.3 Dielectric measurement.....	27
Chapter 6 - Conclusion and Future work .....	29
References .....	30

## List of figures

Fig 1 – Various components of lower sections which includes sample holder, Pt100, cartridge heater, Cu wire, electrical sapphire insulator, specimen, and PCB. (b) Cylindrical lid. ....	4
Fig 2.1 – ABO <sub>3</sub> type Perovskite .....	7
Fig 2.2 – Dipole moment .....	9
Fig 2.3 – Electronic polarization .....	9
Fig 2.4 - The schematic shows the cases without and with external electric field .....	10
Fig 2.5 - The diagram shows orientation polarization without field applied (left) and with applied field (right).....	11
Fig 2.6 – Space charge polarization .....	12
Fig 2.7 – Polarization with and without electric field .....	14
Fig 2.8 – Hysteresis loop .....	15
Fig 2.9 - The diagram shows (A) Direct (B) Converse piezoelectric effects .....	16
Fig 2.10 - Diagram of perovskite structure of BaTiO <sub>3</sub> .....	17
Fig 2.11 - Crystal structure of BaTiO <sub>3</sub> in different phases. (a) Cubic structure (b) Tetragonal (c) Orthorhombic (d) Rhombohedral. ....	18
Fig 3.1 – Autoclave and Teflon container .....	19
Fig 4.1 – XRD experimental setup .....	22
Fig 4.2 – Raman spectroscopy setup.....	23
Fig 5.1 – XRD Plot .....	25
Fig 5.2 – Raman Plot .....	27
Fig 5.3 – Dielectric measurement.....	28



# Chapter 1

## Introduction

In this chapter a varying temperature dielectric properties measuring instrument has been assembled. The sample holder fabricated by Dr. Rohtash kumar in his Ph.D work was used. The work could not be fully completed and demonstrated due to covid-19 restrictions. A LCR meter is used to measure complex dielectric permittivity (both real and imaginary parts). A liquid nitrogen system is used to have dielectric measurement varying with respect to temperature in the range of 77.2 K to 500 K at different frequency. A temperature controller is used to control the temperature variation. Liquid nitrogen system is connected with a computer and measurement data is collected using LABVIEW software. Dielectric measurement is done on varying temperature because ceramic sample change phases on different extent of temperature. Thus it is required for understanding phase transformation. The measurement technique is relatively simple and the results can be used to relate different material properties like mass transport, microstructure properties and defects, rate of chemical reaction.

Measurement in this field had started as lumped circuit approximation in which impedance and admittance were used to analyse the response. With the efforts of Cole and Cole the complex attributes of dielectric permittivity came into picture which is also known as cole - cole plot (real and imaginary parts of dielectric in argand plane). Further smith chart impedance diagram and Nyquist plot were used for impedance measurement. Impedance plane and admittance plane plotting were also done to analyse conductivity in electrolytes. Since then many experimentation has occurred that describes the importance of impedance in dielectric studies.

Dielectric analysis can connect many dots in research and experimentation. It is very useful in conductivity measurement, phase variation, grain boundary and changes occurring along it, ferroelectric properties calculation, defects occurring in crystal lattice, microstructure studies. Future potential of these studies include application in semiconductors, fuel cells, ferroelectric and piezoelectric materials etc.

### 1.1 Impedance spectroscopy

Impedance spectroscopy is a technique for characterising a wide range of electrical properties in materials. It can be used to explain the mechanism of bound or mobile charge in the bulk or interfacial areas of any solid or liquid medium, including ionic, semiconducting, insulator and mixed electronic–ionic conductors.

The common method of measurement is to apply an electrical stimulus (either a current or voltage) and observing the result (voltage or current). Several micro-scopic processes gets activated when an electrical stimulus is applied and in response an electrical quantity either in the form of voltage or current is measured. It includes movement of electron, electron transfer due to interfaces and other atomic variety (may be charged or uncharged) and charge atoms or their agglomerates flow through the defects. The flow rate of charged particles within a material depends upon the ohmic resistance.

There are various types of electrical stimulus in impedance spectroscopy. First method uses transient method in which a step voltage function  $[V(t) = V_0, \text{ for } t \geq 0]$  is applied a  $t=0$  to the system and the time varying current is measured. The ratio  $\frac{V_0}{i(t)}$  is the time varying resistance, which measures the impedance due to step voltage. The results which are time varying in nature is converted into frequency domain through Laplace or Fourier- transform which provides impedance as a function of frequency. The advantages of this method are that it is simple to test. The rate of the reaction is controlled by the independent variable, voltage. The necessity for integral transformation of the data, as well as the fact that the signal-to-noise ratio varies between frequencies, means that the impedance may not be well calculated over the appropriate frequency range, are both disadvantages.

In second method a random white noise is fed and resulting current is measured. Then its Fourier transform is taken to evaluate impedance in frequency domain. Due to short duration of signal in time domain data collection can be done in faster pace. But the disadvantage is that an ideal white noise signal and Fourier transform analysis is required. Sine functions can be used for better signal to noise ratio and linear system response.

The third method, the most general one, measures the impedance by feeding a single frequency voltage or current signal and operating the complex impedance with real and imaginary parts. Most instruments uses this method to determine impedance as a function of frequency and calculations can be easily done by connecting a computer .Easy availability and better signal to noise ratio are its advantages.

The Fourier transform is applicable for linear time invariant system. But most systems are non-linear in nature. So impedance spectroscopy measurement in any of the time or frequency domain is possible only for signals of the magnitude so that the overall system remains linear. As long as the applied voltage remains lower than the thermal voltage,  $V_T = \frac{kT}{e}$ , (k is the



boltzman's constant, T is the absolute temperature in kelvin, e is the fundamental charge value) whose value is approximately 25 mV at room temperature. Till this threshold is not breached the overall system response can be approximated to linear system response. [1]

## **1.2 Specification required for the assembled instrument**

Temperature- In the light of current experiment wide range of temperature is required to observe the phase transformations.so the system's thermal stability is essential(more specifically in the range of 77.2 K to 500 K).

Vacuum level – As the temperature drops the water molecules present in air starts to condense which can cause error in measuring dielectric values. So a specified (In order of  $10^{-3}$  Torr ) vacuum level is required to operate the instrument without having moisture problems .

Computer system –To control and measure the different instrument like LCR meter, Liquid nitrogen system a operating system is required. It can be used to program on LABVIEW to control the functioning of experiment autonomously.

## **1.3 Assembly of liquid nitrogen system**

The Liquid nitrogen system can be divided into three sections for elaborate understanding. There are upper, middle and lower section. Stainless steel alloy and aluminium metal are used for the fabrication of skeleton or structural part of liquid nitrogen system. This liquid nitrogen compatible sample holder was fabricated by Dr. Rohtash as part of his Ph.D Thesis. A brief description of sample holder will be reported here.

The upper section consists of a ten pin connector, ten male-female BNC connectors and one O-ring . The middle section of consists of stainless steel pipe having an outer diameter (OD) ~ 20 mm and length ~ 1 meter. One side of stainless steel pipe is connected through stick welding to a stainless steel flange (upper section) having (OD) ~ 136 mm and length ~ 100 mm, while another side of stainless steel pipe is connected to lower section of the system .The middle section of pipe has a Wilson coupling arrangement which can be used for adjusting the height of liquid nitrogen cylinder and just above the Wilson coupling; a vacuum pipe is connected to the rotary pump for vacuum.

The lower section consists of the sample holder, cartridge heater, a temperature sensor (Pt100), printed circuit board (PCB), cylindrical lid and the electrical sapphire insulator. A thick copper

sheet was chosen for construction of sample holder assembly in the cylindrical shape, having OD and thickness 25 mm and 2 mm, respectively.

#### 1.4 Design and construction of sample holder of lower section

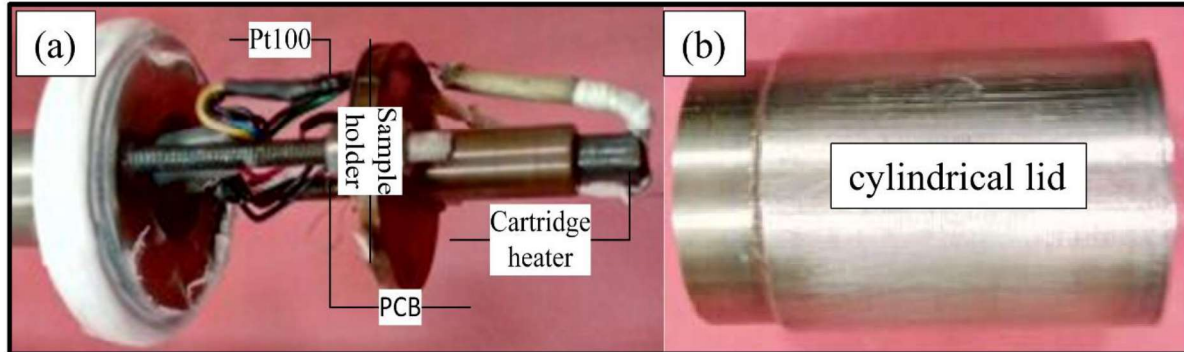


Fig 1 – Various components of lower sections which includes sample holder, Pt100, cartridge heater, Cu wire, electrical sapphire insulator, specimen, and PCB. (b) cylindrical lid.

Copper materials were used to construct the sample holder for dielectric permittivity measurement because of good conductivity. A thick copper sheet was chosen for the construction of sample holder in the cylindrical shape, having OD and thickness 25 mm and 2 mm, respectively. A hollow copper tube ~ 35 mm in length and OD ~ 1 mm is attached at the lower end of the thick circular (Cu) plate. A cartridge heater (OD ~ 0.9 mm) is inserted into the hollow tube. The sample holder contains four small holes. Two holes are used for attaching the holder to the flange in lower section using screws. The remaining two holes are used for electrical connection to cartridge heater. An epoxy fixes the temperature sensor just near the specimen at the centre of the sample holder.

During temperature-dependent property measurement, we observed that sample holder with moderate thickness (~ 1.5 mm) is most appropriate to work in the temperature range of 0 K to 500 K. A thicker sample holder takes a longer time to heat the material which creates error with respect to measurement along temperature. On the other hand if the sample holder is thinner it gets heated and cool down very quickly. So that it can keep up with the desired rate of temperature change and any deviation in measurement can be minimized.

#### 1.5 Vacuum system accessory

Following accessories were used for the vacuum system: (a) vacuum gauge meter, (b) rotary vacuum pump, (c) vacuum pump pipe, (d) KF coupling with an O-ring. Rotary vacuum pump



was used in our experiment to decrease the pressure inside the liquid nitrogen system upto the desired level (in the order of  $10^{-3}$  Torr).

### **1.6 Measurement procedure for dielectric properties**

A precision LCR metre (applied r.m.s. voltage signal of  $\sim 1$  V) in the frequency range of 20 Hz – 2 MHz was used to evaluate the dielectric characteristics of ceramics samples over a large temperature range of 80 K – 500 K. The following instruments are connected to the LCR metre, are temperature controller, Liquid nitrogen system, and computer through GPIB cables for automated data acquisition using the LABVIEW interface. Before proceeding with the measurement, the LCR metre cable must be calibrated (i.e. open, load and short compensation)

Following are the parts of this measurement set-up: (a) precision LCR meter (Model: E4980A, Agilent Technologies), (b) temperature controller, (c) rotary vacuum pump, (d) GPIB (General Purpose Instrument Bus) cables, I computer interface using National Instruments (NI's), (f) Liquid nitrogen container (capacity  $\sim 10$  or 26 litres), (g) GPIB controller for USB adapter, (h) DIN connector for temperature controller, (i) 10-pin connector or 10-pin electrical feed through, (j) test cable assembly (16048A) is a 4-terminal pair type fixture equipped with four-BNC connectors and (k) co-axial cables

### **1.7 LABVIEW Program**

Laboratory Virtual Instrument Engineering Workbench (LABVIEW) is a graphical and visual programming system that provides layout of hardware, measures the data and processing that data, equipment control, industrial computerization etc. A LABVIEW Program contains front panel and back panel. The front panel shows the input and output of the program while back panel shows the internal circuit of the system. For using LABVIEW program through computer for operating the assembly GPIB cables and GPIB to USB adaptor are required.

GPIB cables are connected to temperature controller and an LCR metre for parallel interfacing. GPIB to USB adaptor connects these two GPIB cables. Finally, the USB adapter is connected to a computer for data point display. The temperature controller and LCR meter (Model: E4980A, Agilent Technologies) both have parallel IEEE-488 and serial RS-232C computer interface features. The IEEE-488 interface is an instrumentation bus with hardware and programming standards that facilitates instrument interfacing. The temperature controller compiles with the IEEE-488 standard and integrates its electrical, mechanical and functional requirements.

## Chapter 2

### Introduction

Perovskite type of structure have drawn wide recognition in the study and research of ferroelectric and piezoelectric phenomenon due to their vast properties in the field of electric, optics, magnetism, mechanics etc. [2] For a long time lead based perovskite ceramic has been centre of research for their stable structure at high temperature, high piezoelectric coefficient ( $d_{33}$ ) and wide temperature range before reaching curie point. Among lead based ceramics  $\text{PbZr}_x\text{Ti}_{1-x}\text{O}_3$  (PZT,  $d_{33}= 600\text{pC/N}$ ) had been widely used in different type of application like switching, sensing, energy conversion. But due to volatile nature of lead while sintering the composition changes that restrict the synthesis. Other than that lead is causing grave environment problems due to its leaching in ground during both production and disposal. [3 – 5]

This caused a need of lead free ceramic materials to be developed to address the situation on environment as well as on material synthesis sides. But very few materials had promising results as compared to lead based ceramics. Among those  $\text{BaTiO}_3$ ,  $(\text{Bi}, \text{Na})\text{TiO}_3$ ,  $(\text{K}, \text{Na})\text{NbO}_3$  are the materials which have some promising results.[6] Alternatively  $\text{BaTiO}_3$  have shown many characteristics approaching PZT like piezoelectric coefficient ( $d_{33} \sim 190 \text{ pC/N}$ ), electromechanical coupling ( $k_p \sim 0.5$ ). But relatively low dielectric permittivity and piezoelectric coefficient ( $d_{33}$ ) restrain the adoption of lead free piezoceramics. Co-doping of Barium and Titanium with calcium and zirconium respectively has led to high piezoelectric constant ( $d_{33} = \text{upto } 620\text{pC/N}$ ) and dielectric constant ( $\epsilon_r = \text{upto } 18000$ ) and coefficient electromechanical coupling ( $K_p \sim .45$ ) which are comparable to lead based materials. [7 – 11]

But most of material synthesis include solid state method which causes non- homogeneity in structure, high sintering temperature, non-stoichiometric ratios among others. BCZT synthesis through hydrothermal route can compensate the above mentioned problems. The removal of calcination process and lower sintering temperature need can provide an impetus for one step towards efficient industrial production. A wide comparison based on microstructure study, grain boundary, and grain size among others between hydrothermal and solid state route can throw more light on subject matter. [12]



## 2.1 Perovskite Structure

Earlier mineral  $\text{CaTiO}_3$  was known as perovskite, but now it represents a large family of compounds. In general the crystal structure of perovskite is  $\text{ABX}_3$ . Mostly X is oxygen ion but it also include fluorine or chlorine ion. The crystal structure is best represented as cubic unit cell in which bigger cations (A) on the corner of the cell and smaller cations (B) on the body centre of the unit cell with oxygen occupying centre of the face of the cell.

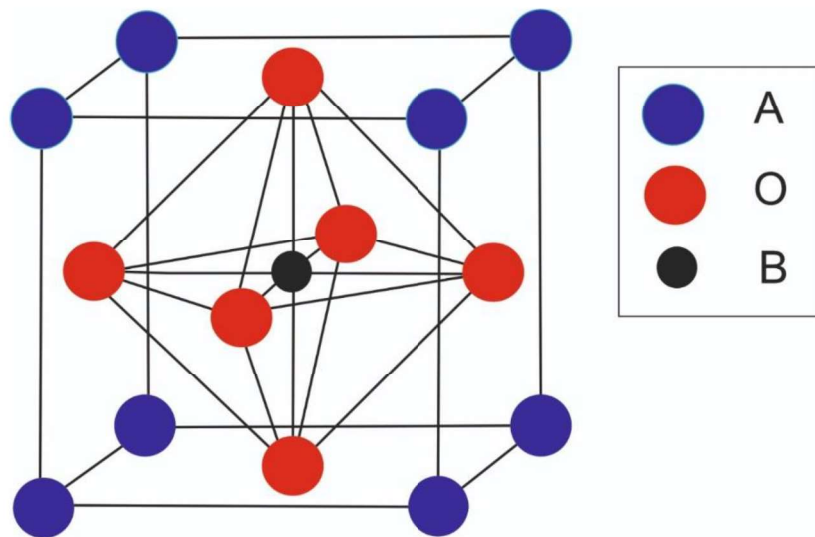


Fig 2.1 –  $\text{ABO}_3$  type Perovskite

Other way of describing crystal structure is through a  $\text{BO}_6$  octahedral with A cations having 12 fold coordination location. Ideally it should be symmetric structure but due to distortions caused by temperature or stress it changes its phase among tetragonal, cubic, rhombohedral and orthorhombic. Due to distortions present in crystal structure the material show good dielectric, ferroelectric and piezoelectric properties. With origin lying at the centre of cubic cell, the corner atoms occupy position  $(1/2, 1/2, 1/2)$ , centre atom occupy  $(0, 0, 0)$ , and face centred atoms occupy position  $(1/2, 0, 0)$ ;  $(0, 1/2, 0)$ ;  $(0, 0, 1/2)$ . [13]

Due to distortion and partial replacement of elements at the A and B site give rise to many properties including Dielectric, Optical, Ferroelectricity, Superconductivity, Piezoelectricity, Multiferroicity, Colossal magneto resistance, Catalytic activity.

## 2.1.1 Causes of distortion

### 2.1.1.1 Tolerance effect

If the cubic unit cell has an edge length of 'a' and ionic radii of A B and O are  $r_A$ ,  $r_B$  and  $r_O$  respectively, where

$$a = \sqrt{2}(r_A + r_B) = 2(r_B + r_O)$$

Goldschmidt's tolerance factor (t) can be used to determine the factor of distortion based on ionic radii of different element.

$$t = \frac{(r_A + r_O)}{\sqrt{2}(r_B + r_O)}$$

The value of tolerance factor is less than 1 if A ion is smaller and it greater than 1 if A ion is larger in comparison of B ion. The value is 1 for an ideal cubic crystal structure. Due size mismatch present between ionic radii of A and B ions tolerance factor is not 1 and that leads to presence of different crystal structure like rhombohedral, orthorhombic, and tetragonal. But the tolerance factor only provides rough picture.

### 2.1.1.2 Jahn-Teller effect

This is phenomenon by which a geometric distortion takes place in order to lower the energy and lower the symmetry of complexes. Whenever the  $e_g$  orbital is unsymmetrically filled there is further splitting of these energy level occurs that is  $e_g$  and  $t_{2g}$  further splits. Also this unsymmetrically filled orbital result in elongation or compression of bonds. This gives distorted complexes. For example  $\text{LaMnO}_3$  shows Jahn-teller distortion due non-symmetric  $e_g$  orbitals which cause expansion in  $\text{MnO}_6$  octahedron.

## 2.2 Polarization

A dipole forms when a positive ( $Q^+$ ) and negative charge ( $Q^-$ ) are separated from each other with a length D. It is denoted by electric dipole moment which is equal to the product of one of the charges and distance between them with a direction from negative charge to positive charge.

$$P = Q \cdot d$$



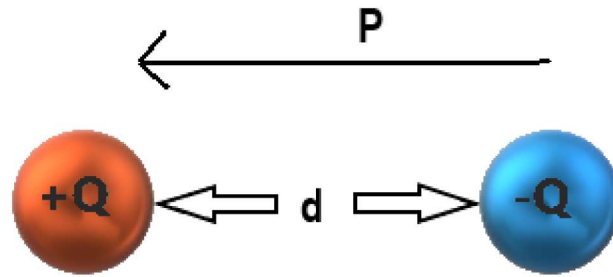


Fig 2.2 – Dipole moment

From Poisson's equation which describes free charge as cause of dielectric displacement or space charge density (D)

$$\text{div } D = \rho$$

For a dielectric material this equation adds two component of electric field. One which was external and other is internal that got generated due to external.

$$D = \epsilon_0 \cdot E + P$$

$$P = \epsilon_0 \chi_e E = \epsilon_0 (\epsilon - 1) E$$

## 2.2.1 Types of polarization

### 2.2.1.1 Electronic Polarization

An atom is electrically neutral as it contains same number of electrons and protons. When an externally sourced electric field is applied to it, then a force is applied on the positive core and electron cloud but in the opposite direction. Due to this a separation gets created between the two which had a neutral dipole moment in the absence of electric field. Separation remains until the field is applied

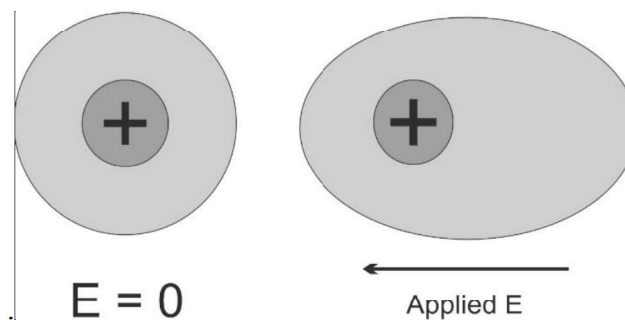


Fig 2.3 – Electronic polarization

As the field is removed the atom comes back to its previous state. Basically the field causes a deformation in the atom which was symmetric earlier. The dipole moment thus generated is directly proportional to electric field applied externally.

$$P = \alpha_e E$$

Where P is dipole moment,  $\alpha_e$  is electronic polarizability with respect to applied field strength E.

### 2.2.1.2 Atomic or Ionic polarization

This kind of polarization is mostly visible in ionic compounds. In polyatomic crystals due to difference in electronegative value a permanent dipole is present. There two groups of ionic solids. One group contain individual dipole moment but due to symmetry the dipole moments get cancelled like NaCl. Thus this group does not have a permanent internal dipole moment. But the second group has individual as well as a net permanent internal dipole moment due to non-symmetric structure like that of HCl.

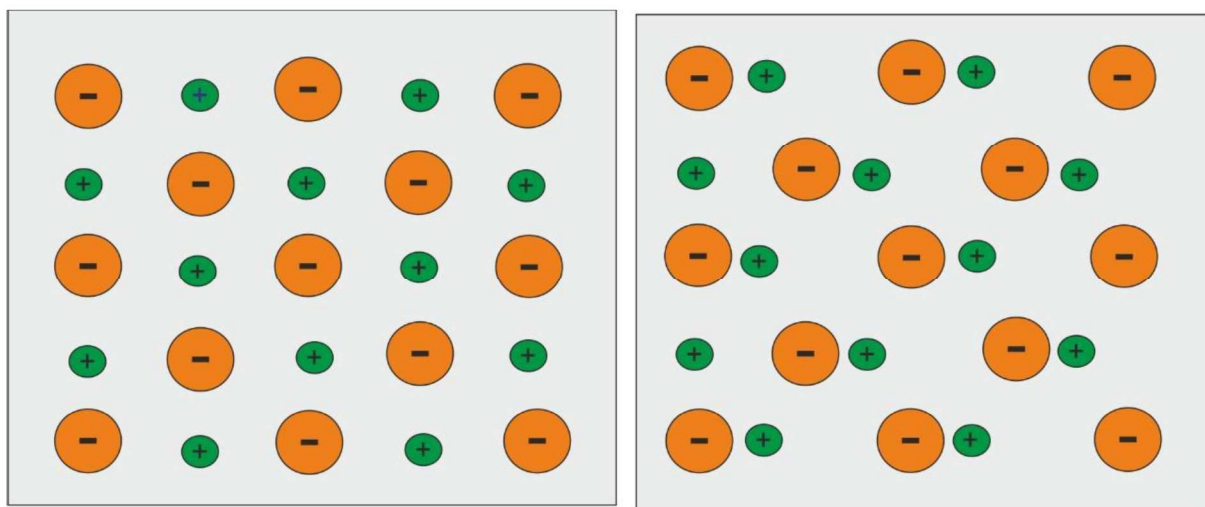


Fig 2.4 : The schematic shows the cases without and with external electric field

When an external field is applied to it the material show net permanent dipole moment because the structure becomes non-symmetric due relatively different movement of cations and anions. This change in separation causes change in bond length that further culminates into dipole moment.

$$P = \alpha_i E$$

Where  $\alpha_i$  ionic polarizability due to field E causing net dipole moment P.

### 2.2.1.3 Orientation Polarization

Unlike ionic polarization, Orientation polarization only occur in the structure which have some net permanent dipole of its own which is present in the absence of any external field. Due to the applied external field the internal dipole moment will position to align in direction of the field. Ex – H<sub>2</sub>O have a net permanent dipole moment due to its asymmetric structure.

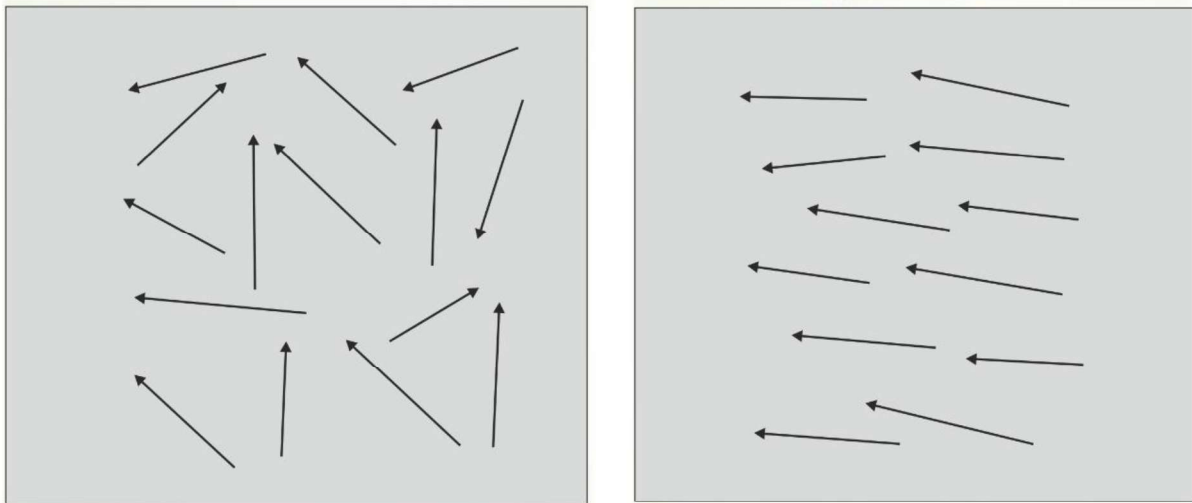


Fig 2.5: The diagram shows orientation polarization without field applied (left) and with applied field (right).

The net polarization of the structure comes back to its original state after the external field is removed. In this polarization energy is required for overcoming the resistance offered by adjoining molecules, so the orientation mechanism is temperature dependent.

### 2.2.1.4 Spontaneous Polarization

This kind of polarization is present in only those crystal structure which does not have centre symmetry. Because in only these structure the centroid of positive and negative charges does not coincide. In ferroelectric materials, polarization take place transition of phase at some certain temperature called as Curie temperature without any application of external electric field. At and above Curie temperature the material generally changes its phase from a polar to a nonpolar phase. Ex – BaTiO<sub>3</sub> exhibits spontaneous polarization. When the temperature is greater than Curie temperature, its structure is cubic which is centrosymmetric. Thus it does not show any spontaneous polarization. But as its temperature decreases below Curie temperature its structure get distorted and changes into tetragonal which is non centrosymmetric. Thus showing spontaneous polarization. Each unit cell carries a dipole



moment reversible in nature along the same direction of neighbouring cell. The series reaction is known as spontaneous polarization.

When an external field is applied the dipoles will position to align in its direction. Upon removal of the field the net dipole moment prevails which was present before application of the field.

### 2.2.1.5 Space charge polarization

The polarization occurs in the presence in presence of mobile or confined charges. Various charge carriers which include ions, electrons and holes which can be injected from interfaces of contacts or may confined in interfacial region. Thus space charges get formed which distort the structure.

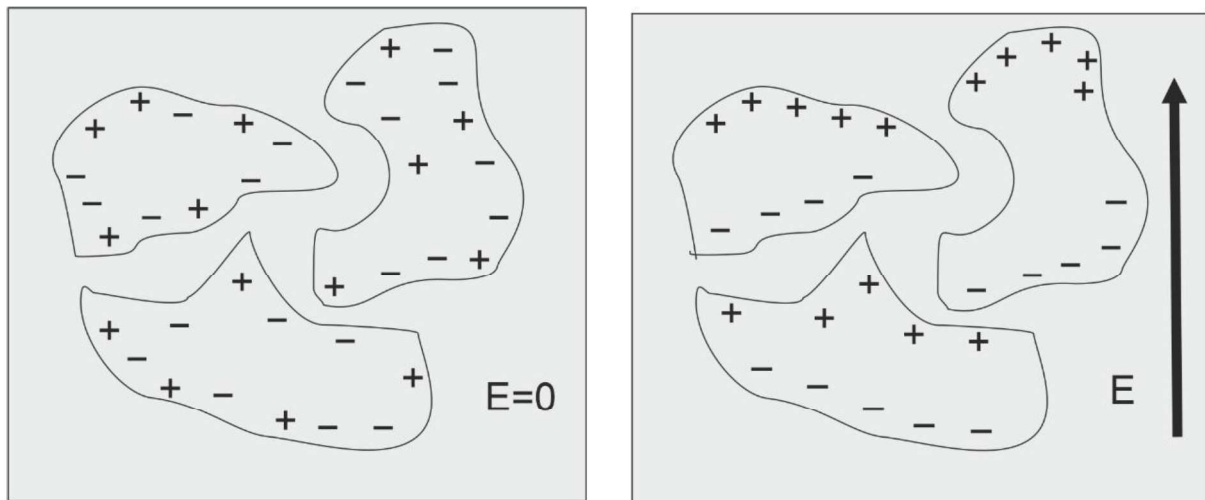


Fig 2.6 – Space charge polarization

In the structure of dielectric, confined charges like ions, electron, holes and vacancies jump from one position to other giving rise to hopping polarization. The charges are able to translate from one site to another for a small time until they get confined or localised. Depending on potential barrier the charge particles can hop or tunnel from one location to other. The dipole is formed due to transfer of charge particle from one to another potential well.

Total Polarizability for dielectric material

$$\alpha = \alpha_e + \alpha_i + \alpha_o + \alpha_s$$

The terms are electronic, ionic, orientation and space charge (which includes interfacial and hopping ) polarizability.[14-15]

## **2.3 Ferroelectricity**

Ferroelectric effect receives its name from the magnetic counterpart Ferromagnetic due to spontaneous behaviour. In ferroelectric materials if an electric field is brought to zero than also polarization does not become zero. A remnant polarization exists in the material. The polarization existing in material is reversible by allowing electric field of value greater than coercive field. But this behaviour cease to exist after reaching Curie temperature. After reaching Curie temperature material attains para-electric phase which is similar to para-magnetic. The non-linearity of polarization with respect to electric field cease to exist in para-electric phase.

There are criteria for materials which show ferroelectric behaviour. First the material must show spontaneous polarization when the electric field is absent. This is present in those of crystalline structures which does not exhibit centre of symmetry. Second is the dipole moment has to be reversible by application of electric field. Among the 32 point groups only 10 show ferroelectricity. The polarization reaction is a hysteresis loop for a ferroelectric material which is a function with respect to electric field. Three variable determine the degree of ferroelectricity which are saturation polarization, remnant polarization and coercive field.

### **2.3.1 Distortion in cubic structure to attain ferroelectricity**

#### **2.3.1.1 Displacement of B cations**

During bringing down the temperature B cations get displaced from the centre of cell to different directions. The displacement in neighbouring cell can be parallel or anti parallel with respect to one another. This give rise to ferroelectric or anti ferroelectric phase. The case in which parallel displacement occurs, the direction of displaced B cations with respect to crystallographic axes give rise to other phases like rhombohedral, orthorhombic and tetragonal.

#### **2.3.1.2 Tilt in octahedral geometry**

Due to the different size of A cations in unit cell and specially in complex perovskites, a tilt in structure occurs in response. This tilt is also included in the estimation of distortion by tolerance factor.

#### **2.3.1.3 Octahedral distortion**

With the help of Jahn-Teller theorem it can be understood that distortion occur due variable bond length on oxygen octahedral structure. The five orbitals of d require a disturbance to the

degeneracy, so as to bring down the energy of the system. In response of this fluctuation in degeneracy causes increase or decrease of bond length of two B-O bonds along similar axis as compared to other four B-O bonds.

### 2.3.2 Domains

The ferroelectric properties are developed in low symmetry phase belonging to 10 group points (which show ferroelectricity). For minimisation of system energy entire volume is sub divided into multiple regions known as ferroelectric domains. Every domain have a characteristic feature that is, all the dipoles are in one direction within on domain may be differing from the orientation of other domains. As every direction is possible orientation, the average within a volume gives zero polarization. The orientation of these domains can be changed with an application of electric field.

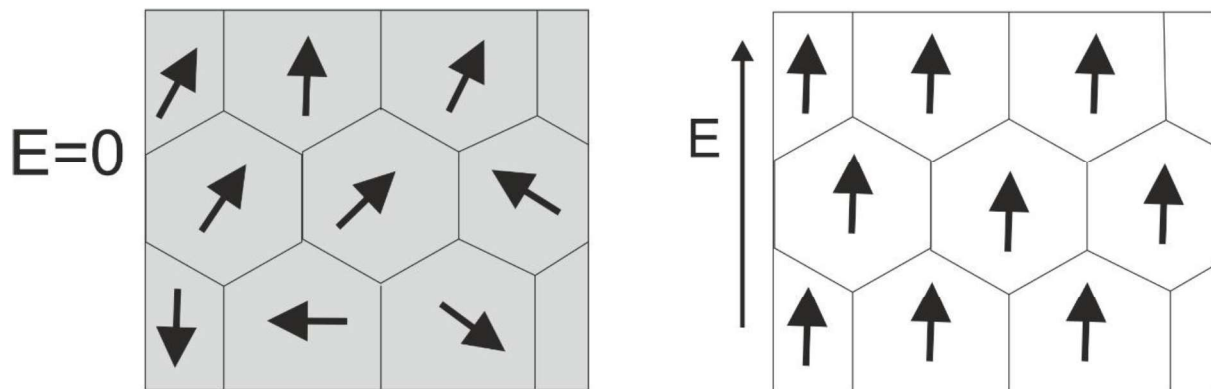


Fig 2.7 – Polarization with and without electric field

Domains are separated from each other through a boundary that make domains distinctive called as domain walls. The domain walls are identified or recognized by the angle between the orientations of dipoles across the boundary. The symmetry is the reason of different direction of polarization which in turn influences and restrict the type of domain walls. During the transformation of phase in a structure, lower the symmetry higher is the allowed orientation states.

Poling is done to align distinct domains orientation in one direction. This results in hysteresis loop of ferroelectric polarization. After poling the ferroelectric material no longer will show zero polarization for zero applied electric field. It will always show polarization even in the absence of electric field. The resultant dipole moment is a dependent upon not only on crystal structure but also on applied electric field. Thus the final polarization is a sum of external as well internal factors. External factor is result of changes in domain orientation due to the



application of electric field after reaching the threshold of coercive field. The internal factor is due to relative movement of charge particles within the structure. This factor is linear in nature and a reversible process while the former one is non-linear in nature and gives hysteresis behaviour. These two components are mutually exclusive and when added changes many properties along with polarization like dielectric and piezoelectric response.

$$P = P_{\text{int}} + P_{\text{ext}}$$

$$\epsilon_r = \epsilon_{r,\text{int}} + \epsilon_{r,\text{ext}}$$

$$d = d_{\text{int}} + d_{\text{ext}}$$

Where p is polarization,  $\epsilon_r$  is dielectric constant and d coefficient of piezoelectricity.[15]

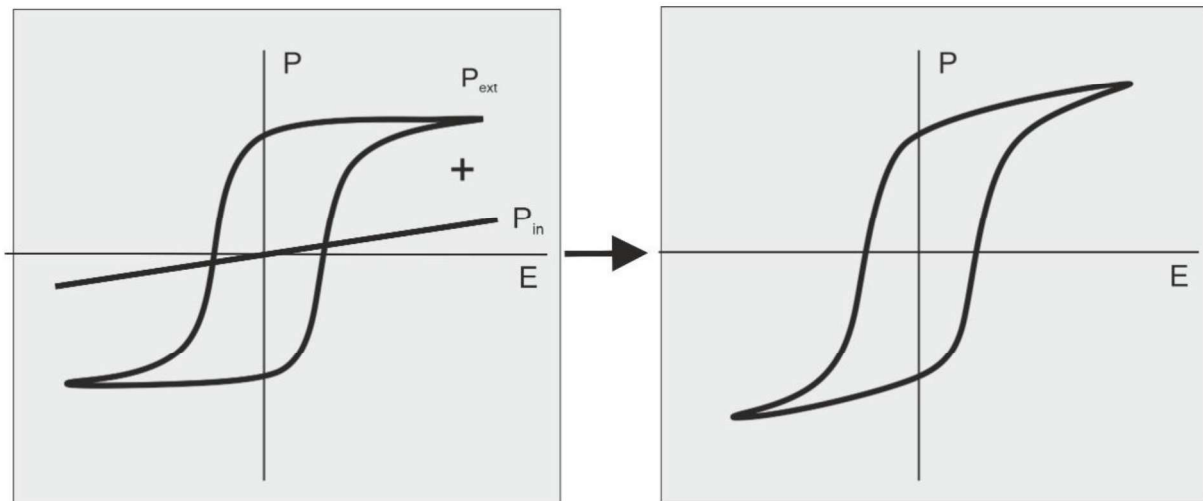


Fig 2.8 – Hysteresis loop

## 2.4 Piezoelectricity

Piezoelectric effect is related with non - centrosymmetric structures and among 32 crystal type only 20 show this effect. Some materials found in nature like quartz shows piezoelectric effect. While materials like PZT, BTO show this effect after poling is done. A perovskite is charge neutral in nature and so does its every unit cell. A mechanical force on the material changes the configuration of B site cations, thus changing polarization effect. This is known as direct effect. Inverse to this when a piezoelectric material is put in electric field, it reacts by changing the position of B site cations leading to more distortion in the cell. All ferroelectric materials exhibit effect of piezoelectricity.

When mechanical strain is exerted on a material showing piezoelectricity, its crystal structure changes giving rise to potential difference in proportion to the pressure applied. To sense the pressure, direct piezoelectricity describes shift in polarization due to the applied pressure as

$$D_i = d_{ij} \sigma_j$$

Where  $D_i$  is dielectric displacement and  $\sigma_j$  is the applied mechanical strain.

Conversely, when an electric field is applied to the material, the change in crystal structure takes place due to change in polarization. Converse piezoelectricity relates the mechanical strain produced in response to an applied external electric field (Actuators).

$$S_i = d_{ij} E_j$$

Where  $S_i$  is resultant mechanical strain,  $E_j$  is electric field applied and  $d_{ij}$  is the coefficient of piezoelectricity.

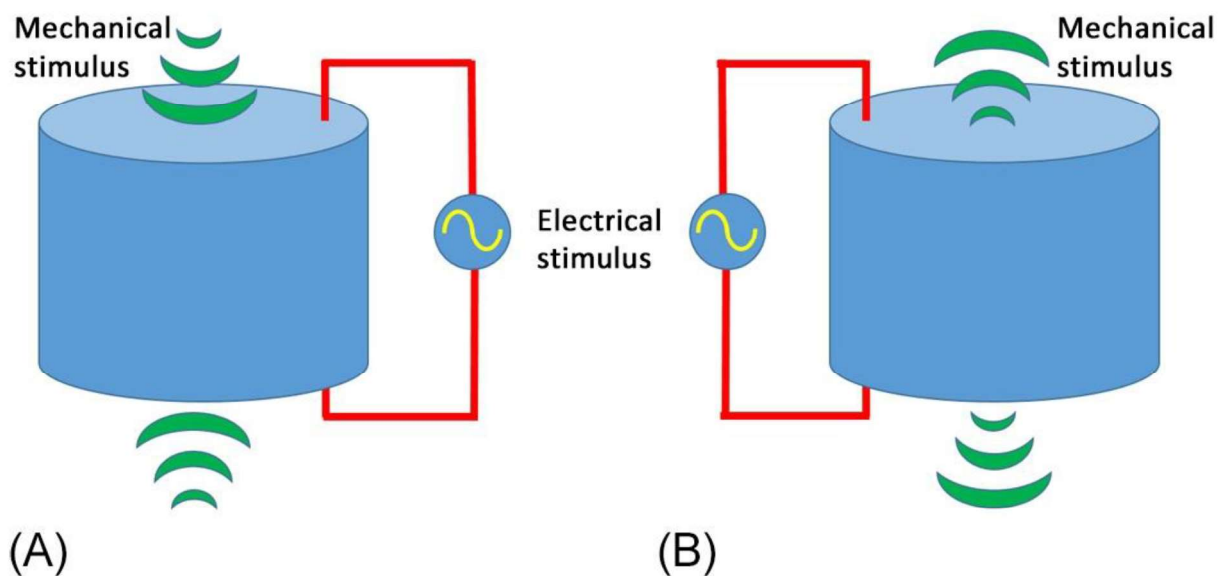


Fig 2.9 : The diagram shows (A) Direct (B) Converse piezoelectric effects [16]

There are multiple domains which are interlinked with one another in a crystal structure of piezoelectric material. Every unit cell contains positive as well negative charge but as a whole it remains neutral. But due to defects or vacancies the charge neutrality for the cell may not hold. But due to symmetric distribution of domains in a crystal, the overall charge is zero. When there is no mechanical pressure on the material, the charges are uniformly distributed giving rise to zero voltage. But due to strain crystal symmetry changes and imbalance of charges create voltage. Potential can be high but the amount of current is small due dielectric

nature of material. In the case of converse process the applied electric field causes disturbance in ions neutral positions leading to distortion in crystal structure and deformation in material.

The coefficient for piezoelectricity ( $d_{33}$ ) is the induced polarization per unit mechanical strain applied, both in the same direction or induced mechanical strain in a direction per unit electric field applied in same direction. And electro-mechanical coupling factor ( $k$ ) provides the convertibility between electrical and mechanical energies of a piezoelectric material. It is the square root of ratio of mechanical energy stored to the electrical energy consumed. [17]

## 2.5 Literature review of BTO

BaTiO<sub>3</sub> was discovered by Wainer and Salomon, Ogawa and Vul in 1942, 1944 and 1944 respectively. It was discovered for its high dielectric permittivity and vast application in capacitors. Since its discovery various research has been going on the dielectric, ferroelectric and piezoelectric properties of BTO. [18] But as compared to PZT its dielectric and ferroelectric properties were inferior and Curie temperature is also lower. In 2009 BCZT, by Liu and Ren was reported which has better ferroelectric, dielectric and piezoelectric properties at Morphotropic phase boundary which can act as a substitute for lead based materials.

### 2.5.1 Structure and phase of BaTiO<sub>3</sub>

Barium Titanate is ABO<sub>3</sub> type perovskite with Ba<sup>2+</sup> occupying the corners, Ti<sup>4+</sup> occupying body centre position and O<sup>2-</sup> located on the face centre of cubic unit cell.

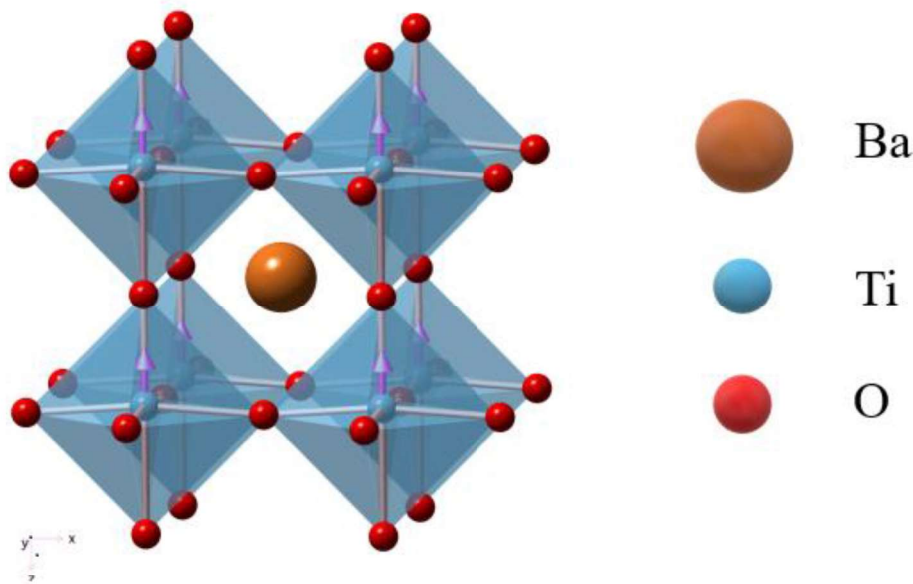


Fig 2.10: Diagram of perovskite structure of BaTiO<sub>3</sub> [19]



At a temperature of approx. 130°C that is known as Curie temperature a phase transition occurs from ferroelectric to para-electric. After Curie temperature the BTO is cubic structure ( $Pm\bar{3}m$ ). For temperature between the Curie temperature and 0°C a tetragonal crystal structure forms due to octahedron disturbance and positive ion moving off the centre of cubic cell. There is a change in positioning of titanium and oxygen ions due to the distortion. Due to asymmetric nature of tetragonal structure, permanent polarization takes along one of the faces of the cell. There are six equivalent  $[100]$  axes direction along which permanent spontaneous polarization can occur when cooled down below Curie temperature.

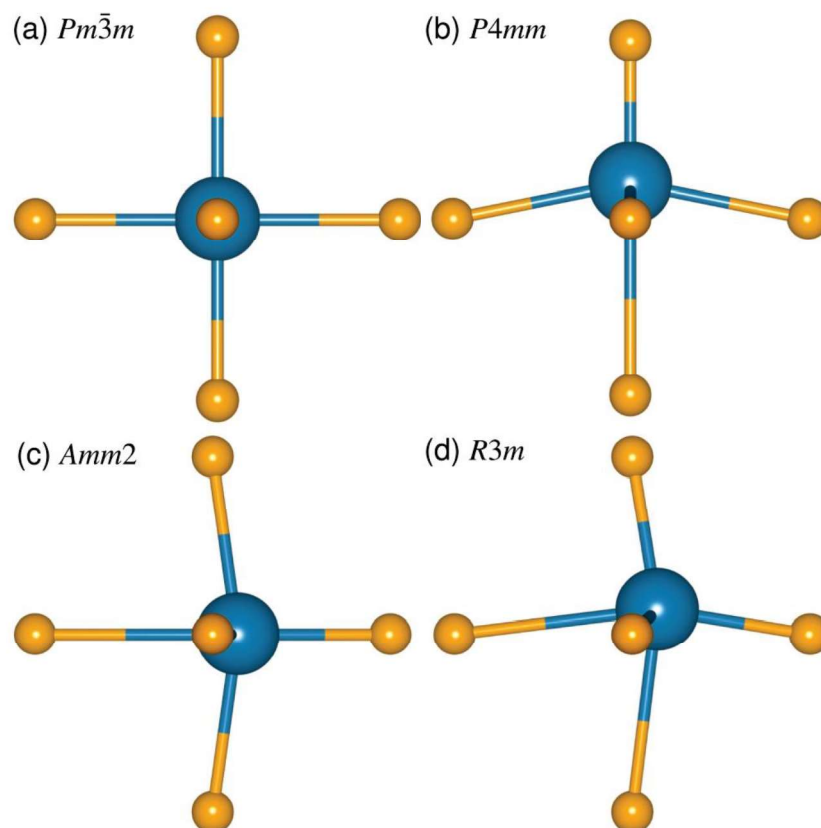


Fig 2.11 : Crystal structure of BaTiO<sub>3</sub> in different phases. (a) Cubic structure (b) Tetragonal (c) Orthorhombic (d) Rhombohedral. [20]

When temperature is even lowered below 0°C, further distortion occur in the tetragonal structure and it changes into orthorhombic ( $Amm2$ ) by lengthening along the direction of face diagonal. There are 12 equally probable  $[110]$  direction in the cubic cell which is also the direction of polarization. Below -90°C the orthorhombic cell goes into another distortion which changes the structure into rhombohedral ( $R3m$ ). There are 8 equally probable directions  $[111]$  along body diagonal which are also direction of polarization. The transition temperature and degree of distortion depends upon rate of cooling, stress and purity. [21]

## Chapter 3

### Synthesis of BaTiO<sub>3</sub>

#### 3.1 Hydrothermal method

This method uses bottom up synthesis model in which compounds dissolved in solvent media (water) combine at molecular level. Method provides a control on the particle size of resultant product. This could be used as an alternative route for nanoparticle synthesis at low temperature as compared to widely used solid state method. In this method the final product precipitates from the solution with temperature being in between of boiling point (100° C) and critical point (374.2° C) in a pressurized autoclave.



Fig 3.1 – Autoclave and Teflon container

Hydrothermal synthesis method has many advantages including relatively low operating conditions (reaction temperatures < 300 °C), single synthesis procedure, environmentally viable due less energy intensive, and good dispersion in solution. [22]

#### 3.2 Experimental synthesis

Ba(OH)<sub>2</sub>·8H<sub>2</sub>O and TiO<sub>2</sub> are used as sources of Ba and Ti respectively for BaTiO<sub>3</sub> synthesis via a hydrothermal route in alkaline medium formed by NaOH. First 2M NaOH was weighed and mixed in water to form a basic solution on a magnetic stirrer. Then Barium and Titanium each of concentration of .5M are weighed and dissolved in the alkaline solution. The mixture is then put into a Teflon container which is then placed inside a stainless steel container.

The container is then put into furnace with temperature at 180° C for 72 hours. The solution was subsequently washed by ethanol and distilled water to remove dissolved impurities. It was then heated for 12 hours at 70° C for obtaining BaTiO<sub>3</sub> powder. [23]



# Chapter 4

## Characterization

### 4.1 X-ray Diffraction

XRD is an essential characterization step for determining the formation, structure, phase, of material. The basis of X-ray diffraction is the constructive interaction between the monochromatic X-rays and sample. Cathode ray tube system (in which accelerated electrons strike the metal plate which acts as anode) is used to produce x-rays, then it is refined to generate monochromatic radiation. Divergence of the beam is kept at minimum to conserve energy. The final radiation generated is the incident to the sample. In general copper targets are used as it produces required radiation  $K_{\alpha}$  with wavelength approximately .154 nm. Applications of XRD include identification of material, determining lattice parameters, characterization etc.

X-ray diffraction is based on Bragg's law. It establishes a relation between the angle at which x- ray is incident towards the sample and the spacing between adjacent planes.

$$n.\lambda = 2d\sin \theta$$

Where n = order of diffraction

$\lambda$  = wavelength

d = spacing between planes

$\theta$  = angle of diffracted radiation

XRD data was collected using Cu- $K_{\alpha}$  source (XRD, Mini Flex, Japan). The scanning rate was adjusted to change at 5° / min within a range of 20° to 80°. [24]



Fig 4.1 – XRD experimental setup

Scherrer's equation provides the average particle size as per given below

$$D = \frac{K\lambda}{B \sin \theta}$$

Where K = shape factor, value close to .9

B = Full width at half maximum (FWHM)

$\lambda$  = wavelength

$\theta$  = Bragg's law. [25]

#### 4.2 Raman Spectroscopy

In 1928, C. V. Raman brought to light the Raman Scattering effect which became the basis of this method of characterization. For a molecule to show Raman Effect, change in polarizability is a must condition. Polarizability is the degree of distortion in electron with respect to its original position. This transitory distortion causes induction of dipole and momentary polarization in molecule. It occurs due to interaction of molecular bond with incident radiation (generally laser). When bond comes back to the normal state, radiation is discharged as Raman scatter.

There are three different type scattering based on elastic or inelastic collision. When elastic collision occurs with the sample then Rayleigh scatter is transmitted in which no transfer of energy takes place. The incident and scattered radiation have same frequency. Due to inelastic

collision stokes and anti-stokes scattering occurs. For stokes scattering, the incident radiation interact with a molecule in ground state for the formation of virtual state. The scattered radiation discharged by molecules reach excited vibrational state of the ground state. The scattered radiation are lower in energy as compared with incident ones. In anti-stokes scattering, the incident radiation interact with a vibrationally excited molecule. The virtual state in this case has more energy than the virtual state generated by excitation of ground state. The scattered radiation generated from the molecules reach ground state. Thus their energy is higher than the ones which were directed towards the sample.

Raman spectroscopy has application in studying molecular structure, bonding characteristics. As molecule's vibrational frequency is unique in nature, the characterization provides data that can identify molecules. It is also used in determining the composition chemistry and structure of the sample material. Enspectra R532 which is a single diode based laser is used for the characterization.



Fig 4.2 – Raman spectroscopy setup



### **4.3 Dielectric Measurement**

The dielectric characterization or spectroscopy is widely accepted and scientific way of determining the electrical properties of ferroelectric materials specially ceramics. The device used is known as impedance analyser. The working of the device is based upon impedance spectroscopy. The device analyses the real and imaginary impedance (L, C, R values) to determine electric permittivity. A.C. measurements over a broad frequency range, in particular, provide valid features of both the bulk and grain boundary dielectric polarisation dynamics. In this experiment real part of electric permittivity is varied along temperature for different frequency electric field. The device has multiple characterisation functions. It can be used to measure ionic conductivity, dielectric loss along with dielectric permittivity measurement. Samples in form of pellets are used in order to measure and electrodes are applied on both sides. The setup required for the measurement consists of temperature controller, furnace and sample holder.

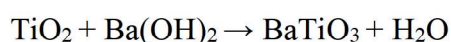
The sample holder contains the sample pellet which is placed inside the furnace. Temperature is varied via temperature controller (Lake Shore 355) connected with thermocouple and impedance analyser(using E4990A (Keysight Technologies)). The temperature controller provide temperature values of sample. Furnace is used to increase the temperature of sample beyond transition temperature. The parameters which are being measured are visible on screen as output. The temperature range chosen for optimum performance is 30-250 °C

## Chapter 5

### Results and discussion

#### 5.1 Structural study

Figure shows the XRD pattern of powder Barium Titanate synthesized via hydrothermal route with  $2\theta$  in the range of  $20^\circ$  C to  $80^\circ$ C. The reaction occurring between Barium hydroxide and Titanium dioxide can be shown as follows:



In the reaction Titanium dioxide concentration starts decreasing and soluble complexes of Titanium hydroxyl starts to form. The complex further reacts with  $\text{Ba}^{2+}$  in the solution to precipitate Barium Titanate. The reaction rate is faster for hydrothermal route due to presence of alkaline medium. The concentration of hydroxyl ion enhances the growth of crystal as  $\text{Ti(OH)}_5^-$  become more soluble in basic condition ( $\text{pH} \geq 11$ ).

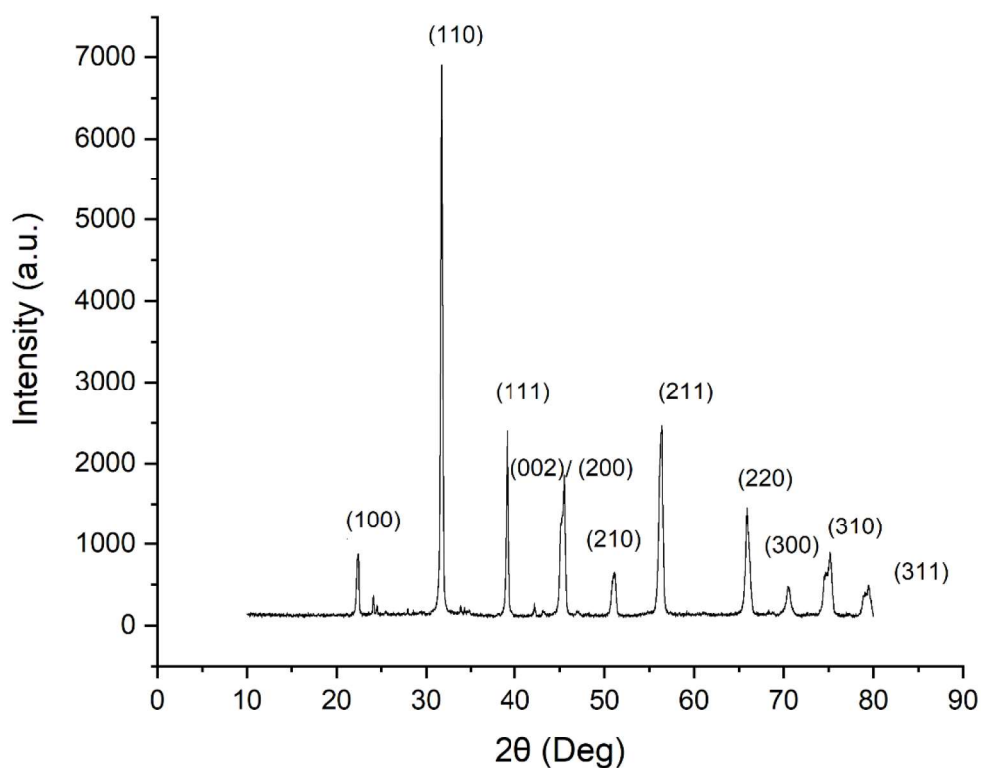


Fig 5.1 – XRD Plot

The material shows mixed phase composed of cubic and tetragonal. The splitting of the (200) peak at  $2\theta = 45.37^\circ$  into two peaks (002) and (200) shows the conversion from cubic to tetragonal. Full width at half maximum (FWHM) and height ratios of peaks for (111) and (002)/(200) determine the distinction between tetragonal and cubic phase. For the tetragonal phase the FWHM for (002)/(200) peak is larger as compared to (111) peak because of the overlapping of earlier peaks with unclear peak bifurcation. Another criterion for tetragonality is that, peak height ratio of (111) and (200) is greater than unity.

Peak	$2\theta$	FWHM	Peak Height
(111)	$39.057^\circ$	0.296	2021.732
(200)	$45.371^\circ$	0.601	1495.158

With the tetragonal major phase of BaTiO<sub>3</sub>, a trace amount of impurity BaCO<sub>3</sub> is also present. The impurity is formed due to reaction between Ba<sup>2+</sup> from precursor and CO<sub>3</sub><sup>2-</sup> from the air. The mean crystalline particle size of Barium Titanate was 19.622 nm, calculated through Scherrer's equation. [26-31]

## 5.2 Raman spectroscopy

The spectrum shows the mixed tetragonal and cubic phase of Barium Titanate. Raman plot also shows the distinction between tetragonal and cubic phases of BaTiO<sub>3</sub>. The peak about 304 cm<sup>-1</sup> and 714 cm<sup>-1</sup> shows the characteristics of tetragonal phase. The peak around 300 cm<sup>-1</sup> has diminishing intensity and it becomes weak if the tetragonal phase is absent or if present is not domineering.

The broader Raman shift peaks about 255 cm<sup>-1</sup> and 519 cm<sup>-1</sup> also shows the Raman peaks present in tetragonal phase of BaTiO<sub>3</sub>. The mentioned Raman shift peaks starts to diminish while reaching Curie temperature and transition to cubic phase. The peaks about 144 cm<sup>-1</sup>, 396 cm<sup>-1</sup> and 639 cm<sup>-1</sup> shows the presence of unreacted TiO<sub>2</sub> (anatase). This shows the incomplete reaction and the quantity is quite low which causes it to remain undetected in X-Ray Diffraction. [32-35]



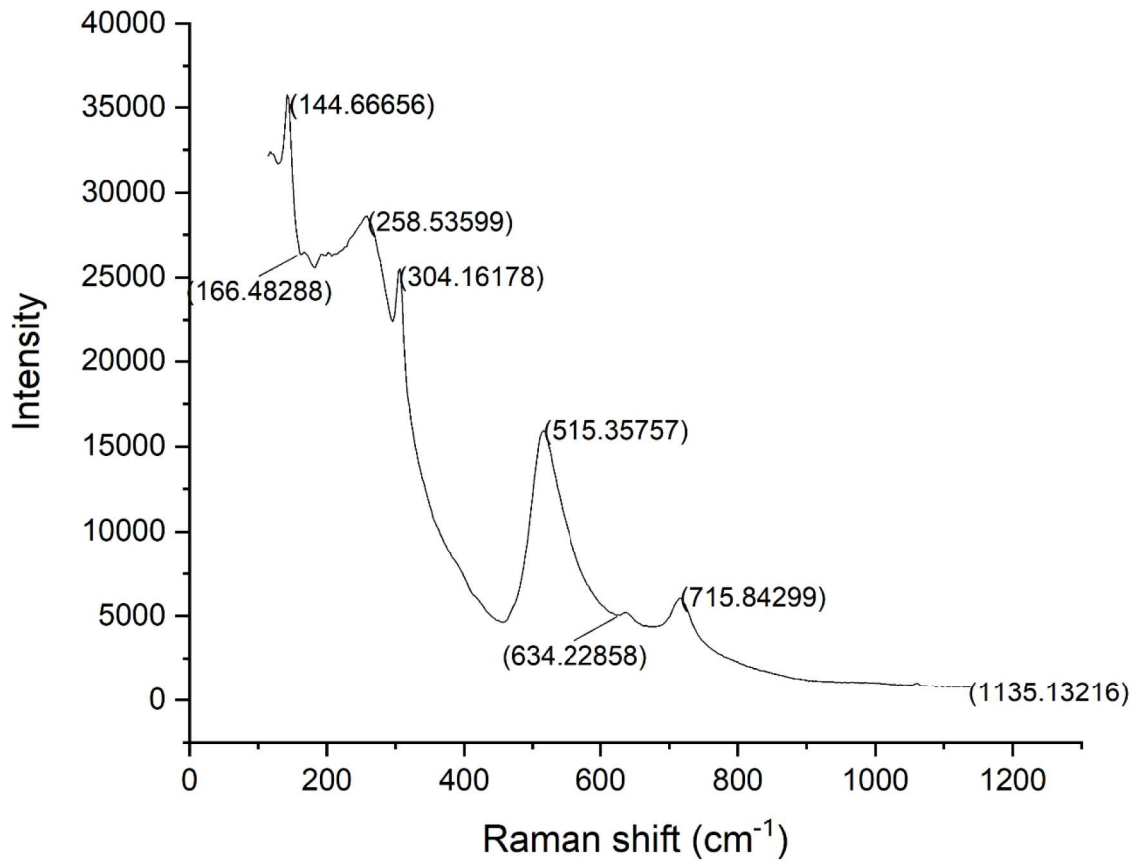


Fig 5.2 – Raman Plot

### 5.3 Dielectric measurement

Dielectric constant of BaTiO<sub>3</sub> sample is measured within the temperature range of 35–250 °C for frequencies 100 Hz, 1 KHz, 10 KHz, 100 KHz, 1 MHz. The dielectric constant increases with increasing temperature till a temperature beyond which the permittivity sharply declines. The temperature on which peak value of electric permittivity is observed is known as Curie temperature. The temperature marks the transition from tetragonal to cubic phase. The transition is also from ferroelectric to para-electric phase. The dielectric constant values are 4507, 3260, 2794, 2522, 2417 for frequencies 100 Hz, 1 KHz, 10 KHz, 100 KHz, 1 MHz respectively. The Curie temperature lies in range of 130 – 132.

It can be observed that the dielectric values decreases as frequency is increased from 100 Hz to 1 MHz. There are four kinds of polarisation present in any material which are electronic, ionic, dipolar, space charge. Electronic and ionic polarization become active at frequencies of order 10<sup>16</sup> and 10<sup>13</sup> Hz respectively. At lower frequencies space charge polarization is

dominant. The saturation of space charge polarization results in declining of dielectric values at high frequencies. Also the decrease in dielectric constant is faster at lower frequencies as compared from higher ones. When frequency applied is increased the dipoles could not keep up with the ac electric field causing decreasing dielectric values. Thus high dielectric values at lower frequencies can be attributed to space charges present. [36-37]

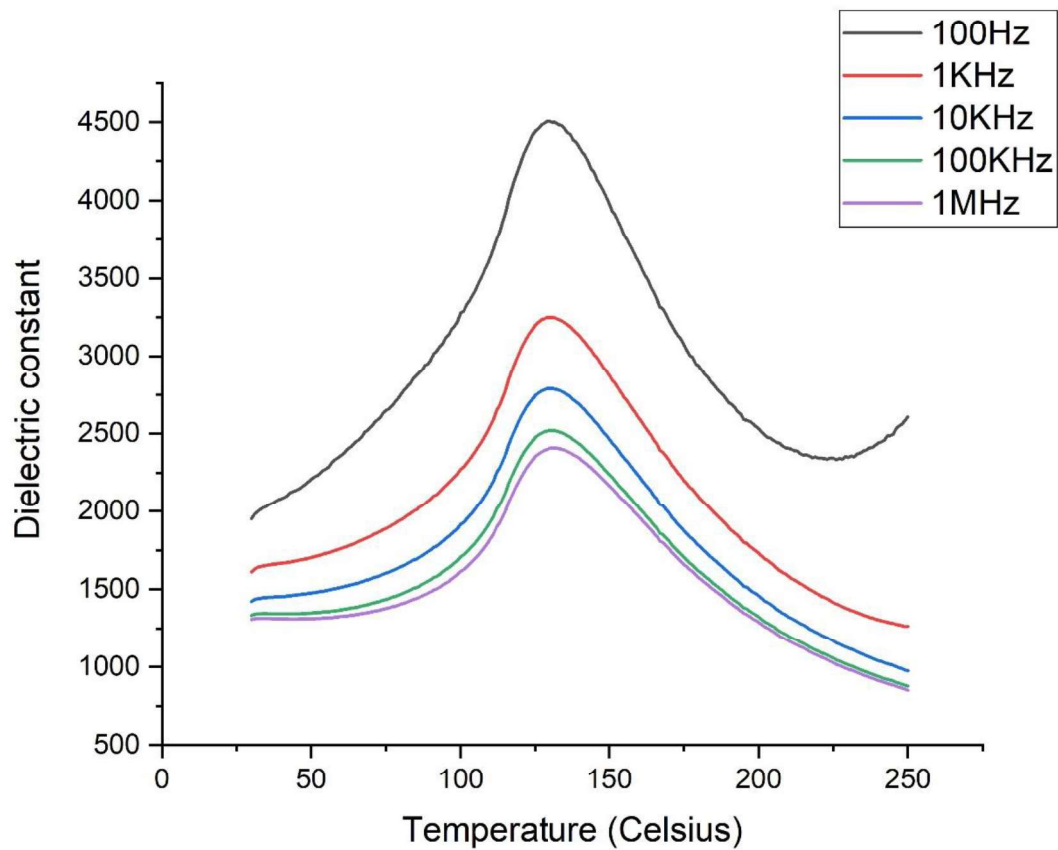


Fig 5.3 - Dielectric measurement

## Chapter 6

### Conclusion and Future work

The thesis provides the apparatus required, principle and method of connecting and installing the dielectric measurement instrument. Impedance spectroscopy provides a back bone for the working of the instrument. LABVIEW program is very useful for obtaining and processing of data gathered. The instrument provides better realisation of material characteristics due to wide range.

The structural study of BaTiO<sub>3</sub> shows both tetragonal and cubic phase. The Bragg's angle range (20° - 80°) conforms the formation of BaTiO<sub>3</sub> via Hydrothermal route. The reaction rate is higher in alkaline medium. The widening of peak near  $2\theta = 45^\circ$  shows the distinction between tetragonal and cubic phase. The particle size is near to 19 nm which conforms nanoparticle formation.

Raman spectroscopy verifies the mixed phase (cubic as well as tetragonal) BaTiO<sub>3</sub>. The peak near to 304 cm and 714 cm shows the characteristic nature of tetragonal phase. Raman analysis shows the presence of TiO<sub>2</sub> which remain undetected in Xrd analysis. While transforming to cubic phase the peaks starts to diminish as compared to tetragonal phase.

Dielectric studies result in rapid change in dielectric values at lower frequencies. As the frequency increases the dependence of dielectric constant on temperature decreases. Space charge polarization caused the dielectric values to increase at lower frequency (4507 at 100 Hz) while its stagnation at higher frequencies caused declining dielectric values (2417 at 1 MHz). Also the ferroelectric to para-electric phase transition occurs at Curie temperature ~ 130 °C.

For future work doping of Barium and Titanium with Calcium and Zirconium respectively, which results in complex perovskite structure can be done. The complex structure shows relatively better properties than parent material in terms of piezoelectricity, ferroelectricity and dielectric properties. Synthesis via hydrothermal provides less energy intensive method with enhanced properties. These material have great application in sensors, actuators, medical instruments and automation.



## References

- (1) Barsoukov, E. and Macdonald, J.R., 2005. Impedance Spectroscopy Theory, Experiment, and Applications, 2nd ed. (Hoboken, NJ: John Wiley & Sons, Inc., 2005).
- (2) Zhang, Y., Deng, H., Si, S., Wang, T., Zheng, D., Yang, P. and Chu, J., 2020. Band gap narrowing and magnetic properties of transition-metal-doped Ba<sub>0.85</sub>Ca<sub>0.15</sub>Ti<sub>0.9</sub>Zr<sub>0.1</sub>O<sub>3</sub> lead-free ceramics. Journal of the American Ceramic Society, 103(4), pp.2491-2498.
- (3) Zhang, Q., Cai, W., Li, Q., Gao, R., Chen, G., Deng, X., Wang, Z., Cao, X. and Fu, C., 2019. Enhanced piezoelectric response of (Ba, Ca)(Ti, Zr) O<sub>3</sub> ceramics by super large grain size and construction of phase boundary. Journal of Alloys and Compounds, 794, pp.542-552.
- (4) Ji, W., Fang, B., Lu, X., Zhang, S., Yuan, N. and Ding, J., 2019. Tailoring structure and performance of BCZT ceramics prepared via hydrothermal method. Physica B: Condensed Matter, 567, pp.65-78.
- (5) Hanani, Z., Mezzane, D., Amjoud, M., Gagou, Y., Hoummada, K., Perrin, C., Razumnaya, A.G., Kutnjak, Z., Bouzina, A., Marssi, M.E. and Gouné, M., 2020. Structural, Dielectric and Ferroelectric Properties of Lead-free BCZT Ceramics Elaborated by Low-temperature Hydrothermal Processing. arXiv preprint arXiv:2011.08100.
- (6) Yang, Y., Guo, J., Ma, W., Zhao, H., Ma, M., Wu, J. and Chi, M., 2019. Effects of V<sub>2</sub>O<sub>5</sub> doping on the structure and electrical properties of BCZT lead-free piezoelectric ceramics. Journal of Materials Science: Materials in Electronics, 30(3), pp.2854-2863.
- (7) Liu, X., Chen, Z., Fang, B., Ding, J., Zhao, X., Xu, H. and Luo, H., 2015. Enhancing piezoelectric properties of BCZT ceramics by Sr and Sn co-doping. Journal of Alloys and Compounds, 640, pp.128-133.
- (8) Lu, X., Fang, B., Zhang, S., Yuan, N., Ding, J., Zhao, X., Wang, F., Tang, Y., Shi, W., Xu, H. and Luo, H., 2017. Decreasing sintering temperature for BCZT lead-free ceramics prepared via hydrothermal route. Functional Materials Letters, 10(04), p.1750046.
- (9) Coondoo, I., Panwar, N., Alikin, D., Bdikin, I., Islam, S.S., Turygin, A., Shur, V.Y. and Kholkin, A.L., 2018. A comparative study of structural and electrical properties in lead-free BCZT ceramics: influence of the synthesis method. Acta Materialia, 155, pp.331-342.
- (10) Hanani, Z., Ablouh, E.H., Mezzane, D., Fourcade, S. and Gouné, M., 2018. Very-low temperature synthesis of pure and crystalline lead-free Ba<sub>0.85</sub>Ca<sub>0.15</sub>Zr<sub>0.1</sub>Ti<sub>0.9</sub>O<sub>3</sub> ceramic. Ceramics International, 44(9), pp.10997-11000.
- (11) Ji, X., Wang, C., Zhang, S., Tu, R., Shen, Q., Shi, J. and Zhang, L., 2019. Structural and electrical properties of BCZT ceramics synthesized by sol-gel-

- hydrothermal process at low temperature. *Journal of Materials Science: Materials in Electronics*, 30(13), pp.12197-12203.
- (12) Ji, X., Wang, C., Luo, W., Chen, G., Zhang, S., Tu, R., Shen, Q., Shi, J. and Zhang, L., 2019. Effect of solution concentration on low-temperature synthesis of BCZT powders by sol–gel-hydrothermal method. *Journal of Sol-Gel Science and Technology*, pp.1-8.
- (13) Smith, M.B., Page, K., Siegrist, T., Redmond, P.L., Walter, E.C., Seshadri, R., Brus, L.E. and Steigerwald, M.L., 2008. Crystal structure and the paraelectric-to-ferroelectric phase transition of nanoscale BaTiO<sub>3</sub>. *Journal of the American Chemical Society*, 130(22), pp.6955-6963.
- (14) Wördenweber, R., 2011. *Ferroelectric Thin Layers*.
- (15) Kao, K.C., 2004. *Dielectric phenomena in solids*. Elsevier.
- (16) Gupta, S., 2021. Introduction to ferroelectrics and related materials. In *Ferroelectric Materials for Energy Harvesting and Storage* (pp. 1-41). Woodhead Publishing.
- (17) Shandilya, Mamta & ShwetaThakur, & Rai, Radheshyam & Singh, Jagtar. (2017). Dielectric relaxation in BATiO<sub>3</sub>-based perovskite.
- (18) Uchino, K., 2017. The development of piezoelectric materials and the new perspective. In *Advanced Piezoelectric Materials* (pp. 1-92). Woodhead Publishing.
- (19) Maraj, M., Wei, W., Peng, B. and Sun, W., 2019. Dielectric and energy storage properties of Ba (1– x) CaxZryTi (1– y) O<sub>3</sub> (BCZT): a review. *Materials*, 12(21), p.3641.
- (20) Page, K., Proffen, T., Niederberger, M. and Seshadri, R., 2010. Probing local dipoles and ligand structure in BaTiO<sub>3</sub> nanoparticles. *Chemistry of Materials*, 22(15), pp.4386-4391.
- (21) Pradhan, S. and Roy, G.S., 2013. Study the crystal structure and phase transition of BaTiO<sub>3</sub>–A perovskite. *Researcher*, 5(3), pp.63-67.
- (22) Ciftci, E., Rahaman, M.N. and Shumsky, M., 2001. Hydrothermal precipitation and characterization of nanocrystalline BaTiO<sub>3</sub> particles. *Journal of materials science*, 36(20), pp.4875-4882.
- (23) Wu, M., Long, J., Wang, G., Huang, A., Luo, Y., Feng, S. and Xu, R., 1999. Hydrothermal synthesis of tetragonal barium titanate from barium hydroxide and titanium dioxide under moderate conditions. *Journal of the American Ceramic Society*, 82(11), pp.3254-3256.
- (24) Epp, J., 2016. X-ray diffraction (XRD) techniques for materials characterization. In *Materials characterization using nondestructive evaluation (NDE) methods* (pp. 81-124). Woodhead Publishing.
- (25) Bhuiyan, M.R.A., Alam, M.M., Momin, M.A., Uddin, M.J. and Islam, M., 2012. Synthesis and characterization of barium titanate (BaTiO<sub>3</sub>) nanoparticle. *Int J Mater and Mec h Eng*, 1, pp.21-24.
- (26) Cho, W.S., 1998. Structural evolution and characterization of BaTiO<sub>3</sub> nanoparticles synthesized from polymeric precursor. *Journal of Physics and Chemistry of Solids*, 59(5), pp.659-666.



- (27) Hongo, K., Kurata, S., Jomphoak, A., Inada, M., Hayashi, K. and Maezono, R., 2018. Stabilization mechanism of the tetragonal structure in a hydrothermally synthesized BaTiO<sub>3</sub> nanocrystal. *Inorganic chemistry*, 57(9), pp.5413-5419.
- (28) Hayashi, H. and Ebina, T., 2018. Effect of hydrothermal temperature on the tetragonality of BaTiO<sub>3</sub> nanoparticles and in-situ Raman spectroscopy under tetragonal–cubic transformation. *Journal of the Ceramic Society of Japan*, 126(3), pp.214-220.
- (29) Hasbullah, N.N., Lee, O.J., Chyi, J.L.Y., Chen, S.K. and Talib, Z.A., 2017. Synthesis of BaTiO<sub>3</sub> nanoparticles via hydrothermal method. In *Solid State Phenomena* (Vol. 268, pp. 172-176). Trans Tech Publications Ltd.
- (30) Pratap, A., Joshi, N.J., Rakshit, P.B., Grewal, G.S. and Shrinet, V., 2013. Dielectric behavior of nano barium titanate filled polymeric composites. In *International Journal of Modern Physics: Conference Series* (Vol. 22, pp. 1-10). World Scientific Publishing Company.
- (31) Hayashi, H., Nakamura, T. and Ebina, T., 2013. In-situ Raman spectroscopy of BaTiO<sub>3</sub> particles for tetragonal–cubic transformation. *Journal of Physics and Chemistry of Solids*, 74(7), pp.957-962.(xrd)
- (32) Ávila, H.A., Ramajo, L.A., Reboredo, M.M., Castro, M.S. and Parra, R., 2011. Hydrothermal synthesis of BaTiO<sub>3</sub> from different Ti-precursors and microstructural and electrical properties of sintered samples with submicrometric grain size. *Ceramics International*, 37(7), pp.2383-2390.
- (33) Kim, Y.I., Jung, J.K. and Ryu, K.S., 2004. Structural study of nano BaTiO<sub>3</sub> powder by Rietveld refinement. *Materials Research Bulletin*, 39(7-8), pp.1045-1053.
- (34) Verma, K.C., Gupta, V., Kaur, J. and Kotnala, R.K., 2013. Raman spectra, photoluminescence, magnetism and magnetoelectric coupling in pure and Fe doped BaTiO<sub>3</sub> nanostructures. *Journal of Alloys and Compounds*, 578, pp.5-11.
- (35) On, D.V., Vuong, L.D., Chuong, T.V., Quang, D.A., Tuyen, H.V. and Tung, V.T., 2021. Influence of sintering behavior on the microstructure and electrical properties of BaTiO<sub>3</sub> lead-free ceramics from hydrothermal synthesized precursor nanoparticles. *Journal of Advanced Dielectrics*, 11(02), p.2150014.
- (36) Sitko, D., Bak, W., Garbarz-Glos, B., Budziak, A., Kajtoch, C. and Kalvane, A., 2013, December. Dielectric properties of BaTiO<sub>3</sub> based materials with addition of transition metal ions with variable valence. In *IOP Conference Series: Materials Science and Engineering* (Vol. 49, No. 1, p. 012050). IOP Publishing.



- (37) Devi, Sheela & Jha, A.K.. (2009). Structural, Dielectric and Ferroelectric Properties of Tungsten Substituted Barium Titanate Ceramics. Asian Journal of Chemistry. 21.